Synthesis, crystal structure, and physical properties of Yb*T*Zn (*T*=Pd, Pt, and Au) and LuPtZn

S. K. Dhar,[1] R. Kulkarni,[1] P. Manfrinetti,[2,3] M. Pani,[2] Y. Yonezawa,[4] and Y. Aoki[4]
[1]*CMP & MS, T.I.F.R., Homi Bhabha Road, Mumbai 400 005, India*
[2]*Dipartimento di Chimica e Chimica Industriale, Università di Genova, Via Dodecaneso 31, 16146 Genova, Italy*
[3]*LAMIA Laboratory-CNR-INFM, Corso Perrone 24, 16152 Genova, Italy*
[4]*Department of Physics, Tokyo Metropolitan University, Hachioji, Tokyo 192-0397, Japan*
(Received 10 April 2007; revised manuscript received 28 June 2007; published 6 August 2007)

We report the synthesis of three new Yb-based equiatomic compounds YbPdZn, YbPtZn, and YbAuZn, and of LuPtZn. According to the results of x-ray diffraction, these four compounds crystallize in the TiNiSi-type structure (orthorhombic *oP*12-*Pnma*, an ordered ternary variant of the Co_2Si type). The Yb ions in YbPdZn and YbAuZn are in the divalent state, while a strong interplay of the single-ion Kondo and magnetic exchange interactions is observed in YbPtZn. The electrical resistivity of YbPtZn increases with decreasing temperature below 300 K, peaks broadly around 45 K, and decreases precipitously below 10 K. A rapidly increasing C_{4f}/T, where C_{4f} is the 4*f*-derived contribution to the heat capacity at low temperatures, indicates the onset of a heavy fermion state which orders magnetically at 1.35 K; a reduced magnetic entropy of just 1.6 J/mol K up to the ordering temperature indicates a small moment state in which the Yb-magnetic moment is appreciably screened by the Kondo interaction. The coefficient of the linear term in the electronic specific heat γ obtained from extrapolating the zero-field data below 0.4 K to $T=0$ K in the magnetically ordered state is 0.75 J/mol K^2, showing a strongly renormalized electronic state due to the Kondo interaction. γ decreases rapidly in applied magnetic fields due to the weakening of the Kondo interaction. The heat capacity and magnetoresistivity data indicate the presence of ferromagnetic correlations between the Yb ions. Such a feature is rare in Yb-based Kondo compounds.

DOI: 10.1103/PhysRevB.76.054411 PACS number(s): 75.30.Mb, 71.27.+a, 75.30.Cr

I. INTRODUCTION

The study of Yb-based compounds is an active area of research in strongly correlated electron systems. The 4*f* shell of trivalent Yb ion is one electron short of full occupation and it is often considered as the hole analog of trivalent Ce ion in which a lone electron resides in the 4*f* shell. Trivalent Yb compounds typically order magnetically at low temperatures, the magnetic coupling between the magnetic moments associated with Hund's rule-derived $^2F_{7/2}$ state of Yb^{3+} ions provided by the indirect, oscillatory Ruderman-Kittel-Kasuya-Yosida (RKKY) exchange interaction. However, in some Ce and Yb based compounds the quantum mechanical hybridization between the 4*f* state of the rare earth ions and the conduction band electron states leads to a strongly correlated ground state, characterized by various anomalies in physical properties such as a strongly renormalized Pauli paramagnetic or a weakly magnetic ground state, enhanced value of the coefficient of the linear term in the heat capacity, a negative temperature coefficient of the electrical resistivity, etc., commonly referred to as heavy fermion behavior.[1] Some of these compounds show the fascinating phenomenon of heavy fermion superconductivity in which the magnetic fluctuations are believed to be the carriers of the pairing interaction between the Cooper pairs. The hybridization in these ambivalent Yb compounds is facilitated by the near degeneracy of the nonmagnetic divalent Yb^{2+}, $4f^{14}$, and the Yb^{3+} states. While the number of cerium compounds showing such anomalous behavior is fairly large, relatively lesser number of analogous Yb compounds is known. The relatively smaller spatial extension of the 4*f* shell in Yb^{3+} ion as compared to that in Ce^{3+} ion, which leads to greater localization and hence lesser hybridization, is one of the reasons. It is, therefore, of interest to identify new Yb compounds and study them for possible heavy fermion behavior. In the past, the understanding of the heavy fermion behavior has benefited from studies on compounds such as $YbCu_4X$ (X=Ag, Au or Pd),[2–4] Yb*TX* (T=Ni,Pd,Pt; X=Sb,Bi),[5–8] $YbCu_4In$,[9] $YbCu_{5-x}Al_x$,[10] $Yb_2T_3X_9$ (T=Co,Rh,Ru; X=Al,Ga),[11–13] etc. More recently, $YbRh_2Si_2$ which undergoes a weak magnetic phase transition at 65 mK and shows non-Fermi-liquid (NFL) behavior in the temperature dependence of its electrical resistivity and specific heat coefficient has been intensively studied.[14–16] Magnetic field induced NFL behavior, ascribed to the closeness of the magnetic ordering temperature to $T=0$ K, has been reported in a YbAgGe single crystal which exhibits two magnetic transitions below 1 K and shows significant anisotropy.[17]

Iandelli and Palenzona have observed that in the binary Yb-*X* systems, the more promising *X* elements to favor a trivalent or a mixed-valent state of Yb are the transition metals belonging to the groups 8–11.[18] A search in the literature showed that no data exist on the occurrence of intermediate phases in the systems Yb-Pd-Zn, Yb-Au-Zn, and Yb-Pt-Zn. Since the 1:1:1 composition is frequently encountered in intermetallic systems, we synthesized the three new equiatomic Yb*T*Zn (T=Pd, Pt, and Au) compounds. The study of their crystal structures and magnetic properties constitutes the subject of the present work; in particular, the presence of a different *T* element provides an opportunity to examine the influence of the *d*-transition metal substitution on the magnetic behavior of the Yb ions. We also prepared LuPtZn as a nonmagnetic reference material for YbPtZn. The magnetic properties of these compounds were probed using the tech-

TABLE I. Thermal treatment and lattice parameters for the *RT*Zn compounds of the present work.

Compound	Thermal treatment	Lattice parameters (Å)[a]			
		a	*b*	*c*	V_{at}
YbPdZn	1123 K 1 week	6.997(1)	4.232(1)	7.942(1)	19.60
YbPtZn	1073 K 1–2 weeks	6.842(1)	4.057(1)	8.103(1)	18.74
LuPtZn	1073 K 1 week	6.816(2)	4.020(1)	8.129(2)	18.56
YbAuZn	1023 K 6 days	7.135(1)	4.456(1)	7.898(1)	20.93

[a]From Guinier powder patterns.

niques of low temperature heat capacity, electrical resistivity, and magnetization.

II. EXPERIMENT

The metals used in the preparation of all the samples were commercial products with high purity: 99.9 wt. % for Yb and Lu, 99.95 wt. % for Pt, Pd, and Au, and 99.999 wt. % for Zn.

All the four compounds were prepared in sealed crucibles, owing to the high vapor pressure of zinc and ytterbium. The weighed amounts of the metals (in the form of surface-cleaned small pieces for Yb and of fine turnings for Lu; 200-mesh powders for Pt and Pd; a 1 mm diameter wire for Au and small chunks for Zn; total mass of about 3 g) were pressed together directly into outgassed tantalum crucibles (wall thickness of 0.5 mm) which were then sealed by arc welding under a pure-argon gas flow. The samples were melted by gradually heating the crucibles twice in a high-frequency induction furnace up to 1500–1600 °C, where they were slightly shaken to ensure homogenization, repeating the procedure twice. For *R*PtZn (*R*=Yb and Lu) samples, a strongly exothermic reaction which takes place when the crucible is heated up to about 800 °C necessitated a gradual and cautious heating up to the highest temperature of about 1600 °C. The slowly cooled crucibles were then sealed under vacuum in quartz tubes and annealed in resistance furnaces at 800 °C for 5–10 days. No contamination of the samples by the container material was noticed.

Metallographic examination was performed by both optical and electron microscopy and semiquantitative phase analyses were performed by microprobe. X-ray investigations were carried out both on powders and single crystals (a small crystallite isolated from the annealed ingot). Powder patterns were obtained by a Guinier-Stoe camera using the Cu $K\alpha_1$ radiation and pure Si as an internal standard (a =5.4308 Å). The observed patterns were indexed by a direct comparison with those calculated with the LAZY PULVERIX program.[19] Intensity data for Rietveld refinement of YbAuZn were collected on a Philips powder diffractometer ($\theta/2\theta$ Bragg-Brentano geometry, Ni-filtered Cu $K\alpha$ radiation) and refined with the DBWS-9807A program.[20] Single crystal data for YbPdZn and YbPtZn were collected at room temperature on a four-circle Bruker-Nonius MACH3 diffractometer, equipped with graphite-monochromated Mo $K\alpha$ radiation (λ=0.7107 Å). In both cases, the diffracted intensities were measured with ω-θ scans exploring one-half of the Ewald sphere (YbPdZn: $\theta_{max}=35°$, $0\leqslant h\leqslant 11$, $-6\leqslant k\leqslant 6$, $-12\leqslant l\leqslant 12$, 2201 total measured reflections, 572 independent reflections; YbPtZn: $\theta_{max}=33°$, $-10\leqslant h\leqslant 10$, $-6\leqslant k\leqslant 6$, $-12\leqslant l\leqslant 0$, 1809 total reflections measured, 473 independent reflections). The structure refinements were carried out by using SHELXL-97,[21] with the following disagreement indices: $wR2=0.074$ ($572F_o^2$, 20 refined parameters), $R1=0.030$ [$534F_0>4\sigma(F_0)$], $S=1.187$, $\Delta\rho_{max}=4.6\ e/Å^3$ for YbPdZn and $wR2=0.010$ ($473F_o^2$, 20 refined parameters), $R1=0.040$ [$388F_0>4\sigma(F_0)$], $S=1.019$, $\Delta\rho_{max}=5.2\ e/Å^3$ for YbPtZn. Further details about the structure refinements are available from the authors on request.

Magnetization was measured in a SQUID (Quantum Design) magnetometer. Heat capacity and resistivity data down to 1.8 K in zero and applied fields up to 12 T were collected using PPMS (Quantum Design). For lower temperatures, the heat capacity was measured by a quasiadiabatic heat pulse method using a dilution refrigerator equipped with an 8 T superconducting magnet. The temperature increment associated with each heat pulse was controlled to about 1%.

III. RESULTS AND DISCUSSION

A. Crystallographic details

All samples were nearly single phase alloys, the parasitic secondary phases contained in grain boundaries being less than 1%–2%.

According to the x-ray diffraction patterns, all the four compounds belong to the orthorhombic TiNiSi type (ternary ordered variant of the Co_2Si structure): the corresponding lattice parameters, as determined by the least-squares methods on Guinier powder data, are given in Table I. The linear trend of $(V_{at})^{1/3}$ vs r_R^{3+}, where V_{at} is the mean atomic volume (cell volume divided by the total number of atoms in the unit cell) and r_R^{3+} the ionic radius of the trivalent rare earth element, along the *R*PtZn series (Fig. 1), indicates the trivalent state of ytterbium in YbPtZn. The two points at the beginning of the RPtZn series correspond to the new TiNiSi-type

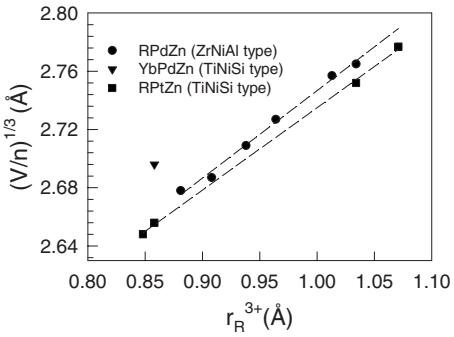

FIG. 1. The cubic root of the mean atomic volumes vs. the atom radii of the rare earths for the two series of equiatomic intermetallics *R*PdZn and *R*PtZn compounds.

homologues LaPtZn and CePtZn, respectively, discovered in the course of this work.[22] The points corresponding to RPdZn series are also shown in Fig. 1. While the compounds with R=Ce,Pr,Sm,Gd,Dy,Er (ZrNiAl type[23]) follow the usual lanthanide contraction, a positive deviation is observed for YbPdZn, in agreement with the divalent behavior of Yb in this compound (see below).

The structural parameters refined from the single crystal data for YbPdZn and YbPtZn, and from powder data in the case of YbAuZn are collected in Table II. The listed atomic coordinates, after standardization with the STRUCTURE TIDY program,[24] show that the ordering scheme is analogous in the three compounds, with the Zn and T (T=Pd, Pt, and Au) atoms always occupying the same positions (in all cases, the exchange between T and Zn led to a significant worsening of the agreement indices). By comparing the observed interatomic distances in the three compounds, it is found that the Yb-Yb distances are not very different, being distributed in partially overlapping intervals. On the other hand, as regards the Yb-T distances, it is worth noting that all the Yb-Pt distances are shorter than the Yb-Pd ones, notwithstanding that the atomic radius of Pt is larger than that of Pd.

A schematic representation of the crystal structure, highlighting the T-Zn sublattice and the connections between the Yb atoms, is shown in Fig. 2.

TABLE II. Atomic coordinates and equivalent isotropic displacement parameters of YbPdZn, YbPtZn, and YbAuZn, all TiNiSi type, qrthorhombic, *Pnma*, *oP*12. All atoms are in Wyckoff position 4*c* with y=1/4.

Compound	Atom	x	z	U_{eq} (Å^2)
YbPdZn	Yb	0.0240(5)	0.68656(4)	0.0113(2)
	Pd	0.2737(1)	0.3839(1)	0.0129(2)
	Zn	0.1509(2)	0.0678(1)	0.0130(2)
YbPtZn	Yb	0.0421(1)	0.6831(1)	0.0106(2)
	Pt	0.2514(1)	0.3756(1)	0.0105(2)
	Zn	0.1357(3)	0.0620(3)	0.0121(4)
YbAuZn	Yb	0.0127(2)	0.6932(1)	0.0198(5)
	Au	0.2814(1)	0.3969(1)	0.0285(5)
	Zn	0.1673(3)	0.0734(3)	0.0431(9)

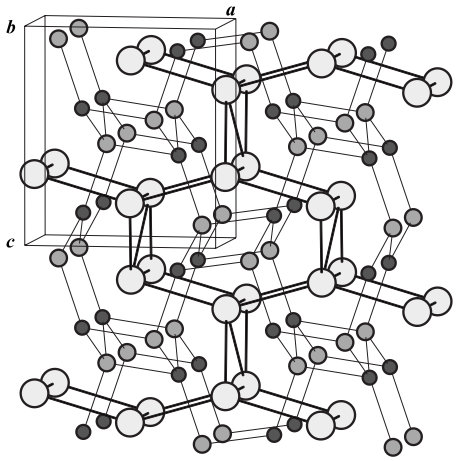

FIG. 2. Crystal structure of the Yb*T*Zn phases (T=Pd,Pt,Au), TiNiSi type; shown are the T-Zn sublattice and the Yb-Yb connections. Large circles, Yb; medium circles, Zn; small circles, Pd, Pt, or Au atoms.

B. Magnetic properties

The inverse susceptibility χ^{-1} of YbPtZn is plotted in Fig. 3. Between 150 and 300 K, χ^{-1} follows the Curie-Weiss relationship given by $\chi=C_{cw}/(T-\theta_p)$, with the effective paramagnetic moment $\mu_{eff}=4.54\mu_B$ (derived from C_{cw}) and paramagnetic Curie temperature $\theta_p=-78.3$ K. μ_{eff} is the same as that for free Yb^{3+}. Though θ_p is large and negative, the data down to 1.8 K do not show any evidence of an antiferromagnetic transition. A large negative θ_p is often observed in Kondo and valence fluctuating compounds and the relations $T_K\sim|\theta_p|/2$ (Ref. 25) and $|\theta_p|/4$ (Ref. 26) have been proposed in the literature. A nearly linear dependence of χ^{-1} vs T below 10 K, when analyzed on the basis of the Curie-Weiss expression, gives $\mu_{eff}=2.4\mu_B$ and $\theta_p=-0.3$ K. The reduced μ_{eff} at lower temperatures can partly be attributed to the crystal electric field splitting, but as we shall see below Kondo screening of the Yb^{3+} magnetic moment is also most likely operative. The in-field magnetization at 1.8 K up to

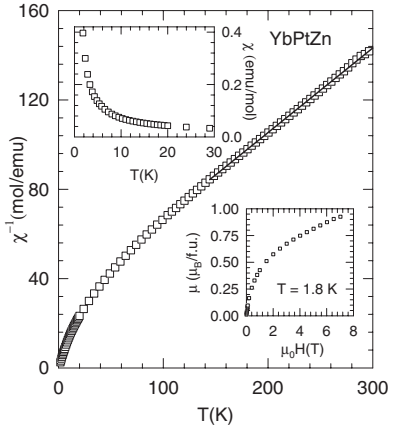

FIG. 3. The inverse susceptibility χ^{-1} of YbPtZn between 300 and 1.8 K. The upper inset shows the susceptibility at low temperatures; lower inset shows magnetization at 1.8 K measured up to 7 T.

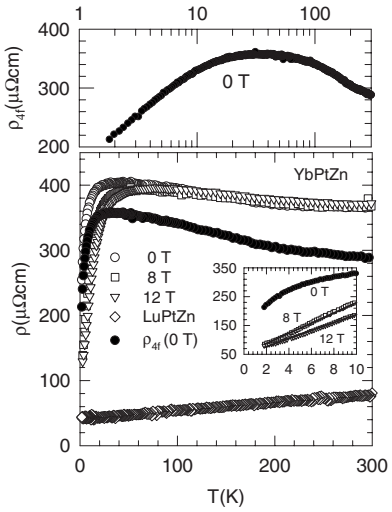

FIG. 4. The electrical resistivity of YbPtZn in zero and applied fields of 8 and 12 T. The resistivity of LuPtZn in zero field and ρ_{4f} ($=\rho_{\mathrm{YbPtZn}}-\rho_{\mathrm{LuPtZn}}$) is also plotted. The inset shows ρ_{4f} vs temperature at 0, 8, and 12 T below 10 K. The solid lines are fits based on a linear variation of ρ_{4f} with the temperature. The top panel shows the plot of ρ_{4f} vs log T.

7 T is shown in the lower inset of Fig. 3. A moment of $0.93\mu_B$/f.u. is obtained at the highest applied field. The deviation of the magnetization from a linear response to the field begins at a low field of 0.1 T. Heat capacity data in applied fields (see below) show that YbPtZn undergoes a magnetic transition at 1.35 K. Therefore, the curvature in the magnetization at 1.8 K may be due to proximity to the magnetic transition. Possible ferromagnetic correlations may also be invoked but a confirmation requires additional magnetization data at lower temperatures.

The electrical resistivity of YbPtZn between 1.8 and 300 K in zero field is shown in Fig. 4. For comparison, the resistivity of the nonmagnetic, reference analog LuPtZn is also shown. While LuPtZn shows metallic behavior, the resistivity of YbPtZn increases below 300 K with decreasing temperature, peaks around 45 K, and then drops precipitously below 10 K down to the lowest temperature of 1.8 K in our experiment. In the applied fields of 8 and 12 T, the peak in the resistivity shifts to higher temperatures. Making the usual assumption that the scattering of charge carriers by phonons in YbPtZn can be taken to be the same as in LuPtZn, we obtain the $4f$ contribution to the resistivity in YbPtZn, ρ_{4f}, by subtracting the resistivity of LuPtZn from that of YbPtZn. ρ_{4f} in zero field is shown in the additional panel to Fig. 4. Between 300 and 90 K, ρ_{4f} shows $a-\ln T$ dependence, which is the hallmark of single-ion Kondo effect. The resistivity data thus show conclusively that YbPtZn is a dense Kondo lattice compound. The decrease of the resistivity below 10 K marks the gradual transition from the single-ion incoherent scattering of the charge carriers to coherent scattering at lower temperatures. It may also be noted that the resistivity data taken at 8 and 12 T show a linear variation with temperature between 1.8 and 10 K (see inset). A linear variation of resistivity with temperature is taken as a signature of the non-Fermi liquid behavior. However, data

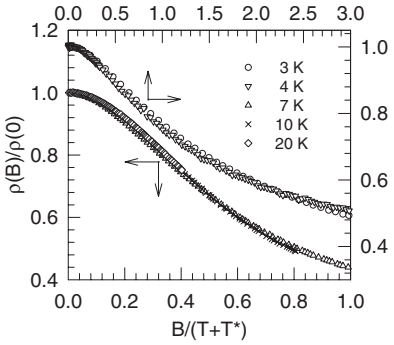

FIG. 5. Normalized magnetoresistance $\rho(B)/\rho(0)$ as a function of $B/(T+T^*)$ at 3, 4, 7, 10, and 20 K (see text for the meaning of T^*).

below 1.8 K are needed to find out whether the observed linear dependence extends down to lower temperatures.

The field dependence of the electrical resistivity at selected temperatures of 3, 4, 7, 10, and 20 K was measured in applied fields up to 12 T and the data are shown in Fig. 5. The negative magnetoresistance decreases with the increase of temperature and is qualitatively typical of the single-ion Kondo effect, the applied field weakening the spin-flip Kondo scattering of the charge carriers. The normalized magnetoresistance for a single-impurity Kondo interaction has been shown to follow a scaling behavior given by $\rho(B)/\rho(0)=f[B/(T+T^*)]$, derived by Schlottmann using the Bethe ansatz to the solution of Coqblin-Schrieffer model, where T^* is an approximate measure of the Kondo temperature.[27] While our data at 7, 10, and 20 K obey the scaling relationship as shown in Fig. 8 with $T^*=0$ K, the magnetoresistivity data at 3 and 4 K are best fit with $T^*=-2$ K. A negative T^* (−0.75 K) was inferred earlier in the heavy fermion superconductor UBe_{13} and attributed to possible ferromagnetic correlations.[28] More recently, Pikul *et al.* have reported a T^* of −1.3 K in the antiferromagnetic ($T_N=5.5$ K) Kondo lattice $CeNiGe_3$.[29] The heat capacity data (see Fig. 6) indicate the presence of possible ferromagnetic correlations in YbPtZn and therefore a negative T^* at 3 and 4 K, in the vicinity of the magnetic transition at 1.35 K, is

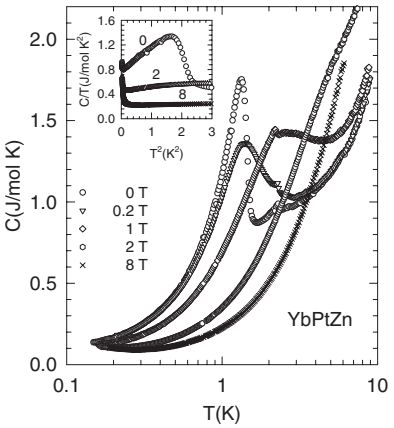

FIG. 6. The heat capacity C of YbPtZn down to 0.15 K in zero and various applied fields up to 8 T. The inset shows C/T vs T^2 at 0, 2, and 8 T.

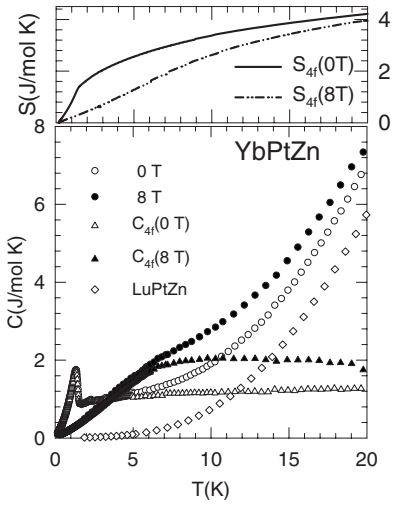

FIG. 7. The heat capacity of YbPtZn up to 20 K in zero and applied field of 8 T. The heat capacity of LuPtZn is also plotted. C_{4f} ($=C_{\mathrm{YbPtZn}}-C_{\mathrm{LuPtZn}}$) in 0 and 8 T is also shown. The entropy S_{4f} obtained by integrating C_{4f}/T with respect to temperature is also shown.

plausible. The net value of T^* may thus arise due to the combined effect of ferromagnetic correlations and the single-ion Kondo effect. At higher temperatures, away from the magnetic transition, the effect of ferromagnetic correlations weakens and T^* increases. A direct correlation of T^* with the single-ion Kondo temperature is thus lacking in the present case.

Figure 6 shows the heat capacity C of YbPtZn between 0.15 and 10 K in zero and various applied fields up to 8 T. The inset depicts C/T vs T^2 at very low temperatures. An anomaly near 1.35 K but with a substantially reduced peak height of just 0.9 J/mol K (compared to the mean field value of 12.5 J/mol K for spin $S=1/2$) suggests a magnetic ordering of low-moment Yb ions. A minor anomaly near 2.2 K arises from the presence of trace amount of Yb_2O_3, which is known to order antiferromagnetically at that temperature. The application of the magnetic field broadens the peak considerably shifting the maximum upward in temperature; an antiferromagnetic transition is typically pushed to lower temperatures in a magnetic field. A similar behavior of the heat capacity in applied fields has been observed in $CeSi_{1.83}$ in which a dense Kondo lattice, ferromagnetic state ($T_c=5.5$ K) has been proposed.[30] In order to derive the $4f$ contribution to the heat capacity C_{4f}, we must have the data for an appropriate nonmagnetic reference analog. LuPtZn was chosen for this purpose and the data for both YbPtZn and LuPtZn up to 20 K in zero and applied field of 8 T are plotted in Fig. 7. The heat capacity of the Lu analog increases monotonically with increasing temperature due to the combined contribution from the lattice and background conduction electron density of the states. C_{4f} is obtained by subtracting the total heat capacity of LuPtZn from that of YbPtZn; i.e., $C_{4f}=C(\mathrm{YbPtZn})-C(\mathrm{LuPtZn})$, making the usual assumption that the lattice heat capacities of isotypic Yb and Lu analog are equal. The plots of C_{4f} in magnetic fields of 0 and 8 T and the corresponding entropies, S_{4f}, are also shown in Fig. 7. C_{4f}/T is 70 mJ/mol K^2 at 20 K indicating a substantial renormalization of the effective electron mass. It increases with decreasing temperature (while C_{4f} is nearly temperature independent down to the ordering temperature) in a fashion similar to that seen in many heavy fermion compounds, in which the large C/T at low temperatures is attributed to the occurrence of Abrikosov-Suhl resonance arising due to the Kondo effect. The entropy S_{4f} attains a low value of 1.2 J/mol K at the transition temperature in zero field, much less than $R\ln 2$ (5.76 J/mol K) for a crystal field split doublet ground state with an effective spin $S=1/2$. Even at 20 K, S_{4f} is 4.2 J/mol K. The behavior of S_{4f} rules out the possibility of a low-lying first crystal field split excited state contributing to a nearly T-independent C_{4f} below 20 K as S_{4f} would then have been larger due to the additional Schottky contribution. The magnetic transition in zero field is sharp and the presence of appreciable short range order above the magnetic transition appears unlikely. Therefore, the substantially reduced heat capacity anomaly associated with the magnetic transition at 1.35 K and a reduced value of the entropy together with the Kondo behavior of the resistivity can be taken to imply a partial screening of the $4f$-derived Yb magnetic moments by the Kondo interaction. The twofold degeneracy of the ground state is partially removed above the magnetic ordering temperature T_m by the Kondo effect. It has been shown that in such cases $S_{\mathrm{mag}}(T_m)=S_K(T_m/T_K)$, where S_K is the entropy at T_m due to the Kondo effect and S_{mag} is the entropy associated with the magnetic ordering.[31] Using Bethe ansatz, Desgranges and Schotte have calculated the entropy and specific heat as a function of T/T_K for a spin 1/2 Kondo impurity.[32] Thus, the ratio T_m/T_K can be determined using the value of S_{mag}. This simple procedure gives T_K to be 9 K, which is consistent with the rapid decrease in the electrical resistivity below this temperature due to the onset of coherence.

In the magnetically ordered state, it is found that C/T at $T=0$ obtained by a linear extrapolation of the zero-field data, from just above the upturn near 0.2 K arising due to the nuclear Schottky contribution, is nearly 0.75 J/mol K^2 (inset, Fig. 6). We infer that the ground state of YbPtZn is characterized by a large Sommerfeld coefficient γ arising from the Kondo interaction. A similar procedure applied to YbPtBi, which undergoes a phase transition at 0.4 K, yielded γ of 8 J/mol K^2.[6] We can derive additional information from the low temperature data by fitting the expression $C(T)=A_N/T^2+\gamma T+c_{\mathrm{mag}}T^n$ to the $C(T)$ data below 0.7 K. The first term corresponds to the nuclear contribution while the last term $c_{\mathrm{mag}}T^n$ is phenomenologically introduced to represent the $4f$ magnetic excitation. The fitted value of n is about 3 in the measured field range, compatible with the excitation of antiferromagnetic spin waves. For a three-dimensional localized-moment ferromagnetic system n is 3/2. However, the contribution of this term to total $C(T)$ at low temperatures is small and its value hardly affects the estimation of γ and A_N as obtained from the fit. The plots of $\gamma(B)$ and $A_N(B)$ vs B ($B=\mu_0 H$) are shown in Figs. 8(a) and 8(b). $\gamma(B)$ decreases rapidly around 1 T and continues to decrease up to 8 T. The application of the magnetic field would tend to break the Kondo coupling between the $4f$ and conduction

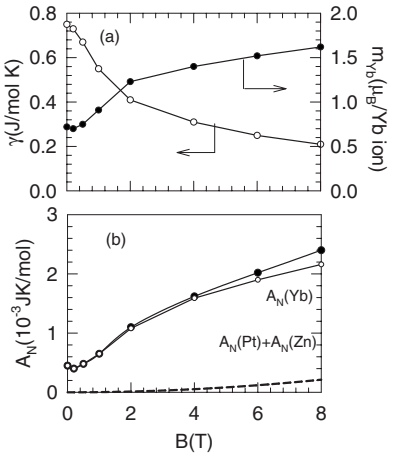

FIG. 8. The plots of Sommerfeld coefficient γ, average Yb magnetic moment, and the nuclear specific heat term A_N as a function of magnetic field.

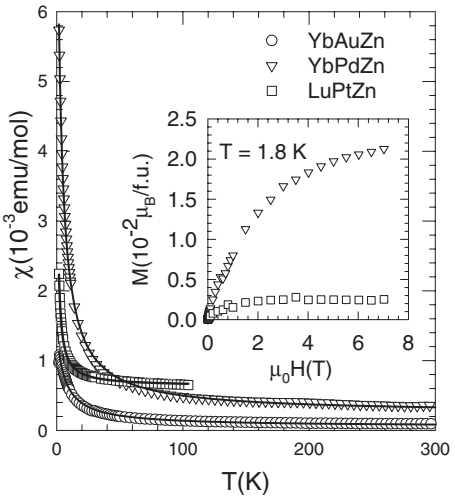

FIG. 9. The thermal variation of the susceptibility of YbPdZn, YbAuZn, and LuPtZn, in the 300–1.8 K range. The inset shows magnetization up to 7 T at 1.8 K.

band electron states and hence reduce γ. The observed $A_N(B)$ can be expressed as $A_N = A_N(\mathrm{Yb}) + A_N(\mathrm{Pt}) + A_N(\mathrm{Zn})$, where $A_N(\mathrm{Pt}) = 1.398 \times 10^{-7} B^2$ (J K/mol) and $A_N(\mathrm{Zn}) = 3.196 \times 10^{-6} B^2$ (J K/mol). Using these values of A_N(Pt) and A_N(Zn), A_N(Yb) can be estimated as $A_N - [A_N(\mathrm{Pt}) + A_N(\mathrm{Zn})]$. A_N(Yb) is further expressed as $A_N(\mathrm{Yb}) = 1.075 \times 10^{-3} (m_{\mathrm{Yb}}/g_J)^2$ (J K/mol), where $g_J = 8/7$ for Yb ion and m_{Yb} is the size of the static, site-averaged Yb magnetic moment at $T < 0.7$ K. Thus, estimated m_{Yb} is shown as a function of B in Fig. 8(a). The zero-field value of m_{Yb} is $\sim 0.75 \mu_B$/Yb ion. This value is much smaller than the full moment of the Yb ion ($4\mu_B$/Yb ion), due both to Kondo screening and the crystal electric field effect such that the doublet ground state has a smaller magnetic moment.

It should be noted that the site-averaged value of m_{Yb} obtained above is the polycrystalline average. Significant anisotropy of the magnetic properties has been reported both in the tetragonal $YbRh_2Si_2$ (Ref. 15) and in the hexagonal YbAgGe.[17] Due to the orthorhombic symmetry of the unit cell, anisotropic magnetic response is expected to occur in YbPtZn as well. Both m_{Yb} and $\gamma(B)$ may show significant variation with the direction of the magnetic field. In YbAgGe, the Kadowaki-Woods ratio A/γ^2 also shows anisotropic field dependence.[17]

An estimate of the characteristic temperature T_0 may be obtained by using the expression $C(T \to 0)/T = \gamma = (\nu - 1)\pi k_B / 6T_0$. This expression was derived by Rajan using Bethe ansatz for solving the exact thermodynamic equations of the Coqblin-Schrieffer impurity model.[33] Taking $\gamma = 0.75$ J/mol K^2 and $\nu = 2$ (the degeneracy of the crystal field split ground state), we obtain $T_0 = 5.7$ K. The characteristic temperature T_0 is related to the conventionally defined single-ion Kondo temperature for $\nu = 2$ by $T_K/T_0 = 1.29$,[34] which implies $T_K = 7.4$ K, in fairly good agreement with the estimate of T_K obtained above from entropy considerations.

An approximate expression for the heat capacity per unit volume due to spin waves in a cubic lattice is given by $C \approx (8\pi^2/15a^3) k_B (k_B T/E_{\mathrm{ex}})^3$ where a is the lattice parameter, k_B is the Boltzmann constant, and E_{ex} is roughly the magnetic exchange energy.[35] Equating the coefficient to c_{mag} obtained above, we infer $E_{\mathrm{ex}} = 5$ K. Keeping in mind that YbPtZn crystallizes in the orthorhombic symmetry with four formula units per unit cell, E_{ex} may be larger. The presence of Kondo interaction reduces the effects of magnetic exchange interaction and YbPtZn orders magnetically at low T_m of 1.35 K with a low Yb magnetic moment.

In sharp contrast to YbPtZn, YbPdZn and YbAuZn behave differently. The thermal variation of the susceptibility of YbPdZn, YbAuZn, and LuPtZn is shown in Fig. 9. The magnitudes of their susceptibilities are comparable showing unambiguously that the Yb ions in these two compounds are in the divalent state. The fully occupied $4f$ shell in Yb^{2+}, like in Lu^{3+}, is nonmagnetic. The in-field magnetization at 1.8 K at the highest applied field of 7 T is small ($\approx 10^{-2} \mu_B$/f.u.), in conformity with the nonmagnetic, ground state of the Yb ions in YbPdZn and YbAuZn. The increase in the magnetization at low temperatures is arising from trace amounts of parasitic secondary phases such as Yb_2O_3 in which the Yb ions are in their trivalent state (see below) and trace amounts of paramagnetic rare earth ions which may be present in $3N$ pure Yb and Lu used in these compounds. Assuming the low temperature upturn in the two Yb compounds is entirely due to Yb_2O_3; we derive presences of nearly 0.34% and nearly 1% of Yb_2O_3 in YbAuZn and YbPdZn, respectively, using the Curie-Weiss expression which includes a temperature independent, χ_0, term also. A similar procedure was applied to LuPtZn as well where the upturn can be ascribed to the presence of paramagnetic ions in $3N$ pure Lu. The "effective Curie constant" proportional to the impurity concentration is the least in LuPtZn, as expected. The curves obtained from the least-squares fitted values are also plotted in Fig. 9. The presence of these trace magnetic pollutants is also reflected in the weak field dependence of the magnetization at 1.8 K. At room temperature, the measured susceptibility of YbPdZn is about 3.7 times larger than that of YbAuZn (χ_0 obtained from the fit above is about an order of magnitude larger for YbPdZn compared to its value in YbAuZn), which can partly be attributed to a higher conduction electron density of states

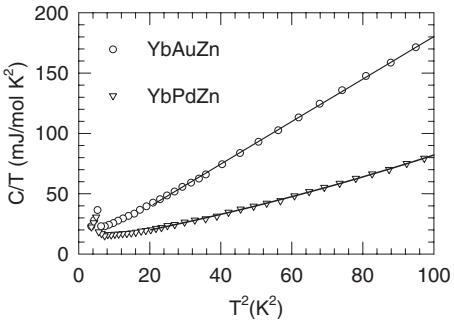

FIG. 10. Low temperature heat capacity of YbAuZn and YbPdZn, plotted as C/T vs T^2.

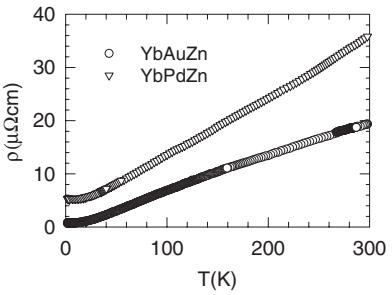

FIG. 11. The electrical resistivity ρ of YbAuZn and YbPdZn from 300 down to 1.7 K.

in the former (see below) and to a larger diamagnetic contribution to the susceptibility in the latter compound; Pd and Au being 4*d* and 5*d* atoms, respectively.

The divalent character of the bulk Yb ions in these two compounds is further corroborated by the low temperature heat capacity data plotted as C/T vs T^2 in Fig. 10. In YbAuZn, a fit of the expression $C/T=\gamma+\beta T^2$, where γ is the Sommerfeld coefficient and β the coefficient of the lattice heat capacity, to the data between 20 and 100 K^2, gave $\gamma=4.2$ mJ/mol K^2. The corresponding value of γ in YbPdZn is 8.8 mJ/mol K^2, obtained after an additional term, δT^4, is added to the fitting expression to account for a slight curvature in the C/T vs T^2 plot. On per gram atom basis, γ in these two compounds is comparable to those of simple metals. The larger value of γ in YbPdZn is in tune with $\chi(\text{YbPdZn})>\chi(\text{YbAuZn})$, as shown in Fig. 9. It may be recalled that in the free electron model, both χ and γ are proportional to the density of states at the Fermi level. The heat capacity of both the Yb compounds shows a small peak near 2.2 K, which arises due to the antiferromagnetic ordering of a trace amount of Yb_2O_3 present in these samples. For LuPtZn (the data are shown in Fig. 7), $\gamma=4.3$ mJ/mol K^2.

The electrical resistivity ρ of YbPdZn and YbAuZn is shown in Fig. 11. A normal metallic behavior is seen, unlike the Kondo behavior in YbPtZn, and ρ decreases with temperature in the entire range from 300 down to 1.8 K. The residual resistivity ratios (RRR) defined as $\rho(300\text{ K})/\rho(1.8\text{ K})$ is 25.9 and 6.75 in YbAuZn and YbPdZn, respectively.

In the TiNiSi-type structure of the YbTZn compounds, the nearest neighbors of Yb ions are the transition metal T atoms. The Yb-T distances are the shortest in YbPtZn. This is in conformity with the nearly trivalent nature of the Yb ions whose ionic radius is smaller in comparison with that of divalent Yb. The cell volume of YbPtZn is also the smallest of the three compounds. The larger Yb-Au bond length compared to Yb-Pd can be attributed to the larger atomic radius of Au, as Yb is in a divalent state in both YbPdZn and YbAuZn. The increase in the valence of Yb on replacement of the 5*d* Pt by the neighboring Au atom can be rationalized on the basis of the tight binding approximation as Au with one extra electron will raise the Fermi level such that the divalent $4f^{14}$ state of the Yb ions is occupied in YbAuZn. In the isostructural analog YbAuSn, Yb retains it nonmagnetic, $4f^{14}$ electronic state.[36] The presence of Kondo interaction in YbPtZn indicates that the Yb-4*f* level is in close proximity to the Fermi level in this compound. The low value of T_K and near equality of the Kondo and magnetic exchange interaction energies result in a robust interplay between the single-ion Kondo and intersite RKKY exchange interactions. Solid solutions of YbPtZn with the Pd and Au analogs provide an opportunity to study the vanishing of magnetic order accompanied with a possible emergence of quantum critical point and NFL behavior. We plan to commence such studies in near future.

[1] For a review, see N. Grewe and F. Steglich, in *Handbook on the Physics and Chemistry of Rare Earths*, edited by K. A. Gschneidner, Jr. and L. Eyring (North-Holland, Amsterdam, 1991), Vol. 14, p. 343.
[2] C. Rossel, K. N. Yang, M. B. Maple, Z. Fisk, E. Zirngiebl, and J. D. Thompson, Phys. Rev. B **35**, 1914 (1987).
[3] P. Schlottmann, Phys. Rev. B **46**, 217 (1992).
[4] P. Schlottmann, J. Appl. Phys. **73**, 5412 (1993).
[5] S. K. Dhar, N. Nambudripad, and R. Vijayaraghavan, J. Phys. F: Met. Phys. **18**, L41 (1988).
[6] Z. Fisk, P. C. Canfield, W. P. Beyermann, J. D. Thompson, M. F. Hundley, H. R. Ott, E. Felder, M. B. Maple, M. A. Lopez de la Torre, P. Visani, and C. L. Seaman, Phys. Rev. Lett. **67**, 3310 (1991).
[7] S. K. Dhar, S. Ramakrishnan, R. Vijayaraghavan, G. Chandra, K. Satoh, J. Itoh, Y. Önuki, and K. A. Gschneidner, Jr., Phys. Rev. B **49**, 641 (1994).
[8] G. LeBras, P. Bonville, J. A. Hodges, J. Hammann, M. J. Besnus, G. Schmerber, S. K. Dhar, F. G. Aliev, and G. André, J. Phys.: Condens. Matter **7**, 5665 (1995).
[9] J. L. Sarrao, Physica B **259-261**, 128 (1999).
[10] E. Bauer, R. Hauser, A. Galatanu, H. Michor, G. Hilscher, J. Sereni, M. G. Berisso, P. Pedrazzini, M. Galli, F. Marabelli, and P. Bonville, Phys. Rev. B **60**, 1238 (1999).
[11] S. K. Dhar, C. Mitra, P. Manfrinetti, A. Palenzonza, and P. Bonville, Physica B **259-261**, 150 (1999).
[12] O. Trovarelli, C. Geibel, B. Buschinger, R. Borth, S. Mederle, M. Grosche, G. Sparn, F. Steglich, O. Brosch, and L. Donnevert,

Phys. Rev. B **60**, 1136 (1999).
[13] S. K. Dhar, C. Mitra, P. Bonville, M. Rams, K. Królas, C. Godart, E. Alleno, N. Suzuki, K. Miyake, N. Watanabe, Y. Önuki, P. Manfrinetti, and A. Palenzona, Phys. Rev. B **64**, 094423 (2001).
[14] O. Trovarelli, C. Geibel, S. Mederle, C. Langhammer, F. M. Grosche, P. Gegenwart, M. Lang, G. Sparn, and F. Steglich, Phys. Rev. Lett. **85**, 626 (2000).
[15] P. Gegenwart, J. Custers, C. Geibel, K. Neumaier, T. Tayama, K. Tenya, O. Trovarelli, and F. Steglich, Phys. Rev. Lett. **89**, 056402 (2002).
[16] J. Custers, P. Gegenwart, H. Wilhelm, K. Neumaier, Y. Tokiwa, O. Trovarelli, C. Geibel, F. Steglich, C. Pépin, and P. Coleman, Nature (London) **424**, 524 (2003).
[17] S. L. Bud'ko, E. Morosan, and P. C. Canfield, Phys. Rev. B **69**, 014415 (2004).
[18] A. Iandelli and A. Palenzona, in *Handbook on the Physics and Chemistry of Rare Earths*, editd by K. A. Gschneidner, Jr. and L. Eyring (North-Holland, Amsterdam, 1979), Vol. 2, p. 1.
[19] K. Yvon, W. Jeitschko, and E. Parthé, J. Appl. Crystallogr. **10**, 73 (1977).
[20] R. A. Young, A. C. Larson, and C. O. Pavia-santos, DBWS-9807°, Rietveld analysis of x-ray and neutron powder diffraction patterns, School of Physics, Georgia Institute of Technology, Atlanta, GA, 2000.
[21] G. M. Sheldrick, SHELXL-97, program for refinement of crystal structures, University of Göttingen, 1997.
[22] P. Manfrinetti (private communication).
[23] A. Iandelli, J. Less-Common Met. **182**, 87 (1992).
[24] L. M. Gelato and E. Parthé, J. Appl. Crystallogr. **20**, 139 (1987).
[25] H. R. Krishna-Murthy, K. G. Wilson, and J. W. Wilkins, Phys. Rev. Lett. **35**, 1101 (1975).
[26] G. Grüner and A. Zawadowski, Rep. Prog. Phys. **37**, 1497 (1974).
[27] P. Schlottmann, Z. Phys. B: Condens. Matter **51**, 223 (1983).
[28] B. Andraka and G. R. Stewart, Phys. Rev. B **49**, 12359 (1994).
[29] A. P. Pikul, D. Kaczorowski, T. Plackowski, A. Czopnik, H. Michor, E. Bauer, G. Hilscher, P. Rogl, and Yu. Grin, Phys. Rev. B **67**, 224417 (2003).
[30] S. K. Dhar, K. A. Gschneidner, Jr., W. H. Lee, P. Klavins, and R. N. Shelton, Phys. Rev. B **36**, 341 (1987).
[31] H. Mori, H. Yashima, and N. Sato, J. Low Temp. Phys. **58**, 513 (1985).
[32] H.-U. Desgranges and K. D. Schotte, Phys. Lett. **91A**, 240 (1982).
[33] V. T. Rajan, Phys. Rev. Lett. **51**, 308 (1983).
[34] N. Andrei and J. H. Lowenstein, Phys. Rev. Lett. **46**, 356 (1981).
[35] A. I. Akhiezer, V. G. Bar'yakhtar, and M. I. Kaganov, Sov. Phys. Usp. **3**, 567 (1961).
[36] D. Kaczorowski, A. Leithe-Jasper, P. Rogl, H. Flandorfer, T. Cichorek, R. Pietri, and B. Andraka, Phys. Rev. B **60**, 422 (1999).